Biosensors and Bioelectronics 126 (2019) 214–221

Contents lists available at ScienceDirect

Biosensors and Bioelectronics

journal homepage: www.elsevier.com/locate/bios

Studies on effectiveness of PTT on 3D tumor model under microfluidic conditions using aptamer-modified nanoshells

Dominika Kalinowska, Ilona Grabowska-Jadach*, Monika Liwinska, Marcin Drozd, Mariusz Pietrzak, Artur Dybko, Zbigniew Brzozka

Chair of Medical Biotechnology, Faculty of Chemistry, Warsaw University of Technology, Noakowskiego 3, 00-664 Warsaw, Poland

ARTICLE INFO

Keywords:
Photothermal therapy
3D cell culture
Spheroids
Lab-on-a-chip
Microfluidic system
Hollow gold nanoshells

ABSTRACT

Herein, we present the research focused on the synthesis and application of aptamer-modified gold nanoshells for photothermal therapy (PTT). NIR-absorbing hollow gold nanoshells were synthetized and conjugated with anti-MUC1 aptamer (HGNs@anti−MUC1). MUC1 (Mucin 1) is a transmembrane glycoprotein, which is over-expressed in a variety of epithelial cancers (eg. breast, lung, pancreatic). In order to evaluate the efficiency of PTT with HGNs@anti−MUC1 we used 3D cell culture model – multicellular spheroids. The selected cell culture model is considered as the best in vitro model for cancer research (similar morphology, metabolite and oxygen gradients, cellular interactions and cell growth kinetics in the spheroids are similar to the early stage of a nonvascular tumor). We conducted our research on human normal (MRC-5, MCF-10A) and tumor (A549, MCF-7) cell lines using a microfluidic system. Aptamer-modified nanoparticles were accumulated selectively in tumor cells (A549, MCF-7) and this fact contributed to the reduction of tumor spheroids viability and size. It should be underlined, that it is the first example of photothermal therapy carried out in a microsystem on multicellular spheroids.

1. Introduction

For many years cancer has been remaining one of the leading causes of human death worldwide (Siegel et al., 2018). The main reason of such a situation is an insufficient effectiveness of anticancer therapies. Moreover, patients are exposed to numerous side effects caused by the most typical treatment methods such as chemotherapy (Babiker et al., 2018) or radiotherapy. Hence, there is an emphasis put on the development of new cytostatic drugs and effective therapies with reduced undesirable effects (Mokwena et al., 2018). To address this concern therapies, which involve light to induce therapeutic effect of antitumor drugs are often employed, e.g. photodynamic therapy (PDT) and photothermal therapy (PTT). However, due to poor tissue penetration by visible radiation (light can penetrate human tissues up to 3 mm), PDT can be applied only to treat a cancer located in areas, which are easily accessible for irradiation such as skin tumors or periodontium diseases (Chifor et al., 2016). It has to be noted, that in the case of PTT near-infrared radiation is applied and penetration depth significantly increased (up to 10 cm depending on the applied wavelength) (Gai et al., 2018). The other crucial requirement for PDT is the presence of oxygen, required to generate reactive oxygen species, which are responsible for the effectiveness of this therapy. Unfortunately, as it is known, the oxygen concentration in solid tumors is limited (this phenomenon is commonly known as hypoxia). Therefore, one has to remember, that this fact may contribute to the reduction of the PDT efficiency. As it was mentioned, PTT due to the application of near-infrared radiation, can be an interesting alternative to PDT therapy. It requires the application of a photoactive agent and its irradiation allow to obtain hyperthermia (ca. 39–45 °C). The selectivity of this therapy is achieved due to the fact that tumor cells are more sensitive to hyperthermia than normal ones (Datta et al., 2015; Ahmed et al., 2015; Mantso et al., 2016; Norouzi et al., 2018). Various materials, e.g. graphene oxide, black phosphorus or MXenes can be used as photoactive agents. Interestingly, gold nanoparticles (GNPs) distinguish themselves with relatively good properties for the application in PTT. The chemical inertness, widely described synthesis methods and simple methods of gold surface modifications result in the frequent application of GNPs in this therapy. It has to noted, that GNPs to be applied in PTT have to absorb the radiation in the near-infrared region. Among these, which are characterized with such a feature, gold nanorods are the most widely applied (Wang et al., 2018; Li et al., 2018). However, their synthesis require the usage of toxic surfactants, which are difficult to be removed

* Corresponding author.
E-mail address: ilona@ch.pw.edu.pl (I. Grabowska-Jadach).

https://doi.org/10.1016/j.bios.2018.10.069
Received 7 September 2018; Received in revised form 19 October 2018; Accepted 31 October 2018
Available online 02 November 2018
0956-5663/

from the resultant solution. The attractive, alternative gold-based nanoparticles, which may be applied for PTT are spherical hollow gold nanoshells (Lopatynskyi et al., 2017) or cubic-shaped gold nanocages (Xia and Xia, 2014), because during their synthesis based on galvanic processes surfactants are not used. The appropriate adjustment of their shape and size allow to obtain NPs, which absorb near-infrared radiation.

In order to study the efficiency of anticancer therapy in vitro, there is a necessity to choose an appropriate cell culture model. Two-dimensional culture models are convenient to set up but do not mimic the tissue microenvironment sufficiently. For example 2D models do not have the typical structure of tumor and there is a lack of typical interactions found in tumor tissue such as: tumor cell-tumor cell, tumor cell-stromal cell and tumor cell-extracellular matrix (ECM) (Weiswald et al., 2015). For this reason 3D cell models are considered as a better reflection of in vivo condition and they become more frequently used for the studies on the efficiency of anticancer therapies. One can find some reports on photothermal therapy conducted on 3D cell cultures in macroscale (Crawford et al., 2017; Gonçalves et al., 2017). However, there is only one report (Min et al., 2017) that describe the application of *lab-on-a-chip* microfluidic system for evaluation of PTT efficiency. The authors proposed a microsystem with channels filled with a hydrogel for co-culturing of two cancer cell lines (human breast cancer MCF−7 and metastatic human glioblastoma U87MG). This device was used for gold nanorod-based photothermal therapy and cell migration studies. Hydrogel allows to obtain 3D cell cultures characterized with the presence of extracellular matrix, that occurs in vivo (Cavo et al., 2018; Gontran et al., 2018). In the case of our work, we decided to carry out the studies on 3D culture, however we selected another model, i.e. multicellular spheroids. Spheroids are good model of early stage of tumors, as in their structure necrotic core and outer layer of proliferating cells can be distinguished. Their formation is stimulated by cells ability to self-organize, when cell-cell interactions are stronger, than interactions between cells and a surface. Some methods for spheroids formation such as: hanging drop, spinner flask method, static liquid overlay technique, centrifugation have been already described (Fennema et al., 2013). However, the method based on the application of microfluidic systems seems to be the most convenient and allow to reduce time-consuming manual steps. In specially designed devices with nonadherent surface spheroids cultures are formed spontaneously after the introduction cell suspension into microchannels. Lab-on-a-chip microsystems are considered to be convenient tools for obtaining and culturing spheroids. They have many advantages as they: mimic in vivo conditions (e.g. simulate the vascular system by laminar flow of culture medium in microchannels, high surface to volume ratio), allow to reduce reagents volumes and increase time- and cost-effectiveness (Kalinowska et al., 2018).

Mucin 1 (MUC1) is a membrane protein, which is presented on the surface of normal cells. It has to be noted, that this protein is overexpressed in many types of cancer cells, including lung and breast ones (Nabavinia et al., 2017). Therefore, mucin 1 is reported to be a target for various anti-tumor treatment strategies, e.g. drug delivery, immunotherapy, radiotherapy, photodynamic therapy (Yang et al., 2018; Singh et al., 2016). Some reports confirmed that MUC1 aptamer-guided photothermal therapy was effective in targeting and killing tumor cells (Azhdarzadeh et al., 2016). However, to the best of our knowledge, no reports regarding application of such a biorecognition agent immobilized on the surface of plasmonic hollow gold nanoparticles have been presented. We decided to use aptamer for nanoshells surface modification, because aptamers have been proven to be attractive substitute to antibodies. It is due to their high chemical stability, low immunogenicity and ease to be used as surface modifiers (Hori et al., 2018). Moreover, it was found (Martinez et al., 2014), that anti-MUC1 aptamers are able to penetrate 3D MCF−7 breast tumor spheroids, while anti-MUC1 antibodies are capable to interact only with the spheroids surface (Martínez et al., 2014).

Herein, we present the studies of the efficiency of photothermal therapy with the use gold nanoshells on spheroids culture in a microfluidic system. It has to be mentioned, that such studies have been carried out for the first time. The designed, synthesized, and surface-modified nanoparticles have been well characterized and their optical and photothermal properties examined. The selectivity of aptamer binding to cell membrane protein (mucin-1) was confirmed. The cytotoxicity of nanoparticles (without exposure to laser irradation) and biological activity after photoactivation (PTT therapy) on normal and tumor spheroids were evaluated.

2. Materials and methods

2.1. Materials

Silver nitrate, gold(III) chloride trihydrate, sodium citrate dihydrate, citric acid, magnesium chloride hexahydrate, sodium borohydride, potassium chloride, tris(carboxyethyl)phosphine hydrochloride (TCEP), 4-(2-hydroxyethyl)−1-piperazineethanesulfonic acid (HEPES) and Tween 20 were purchased from Sigma-Aldrich and used without further purification. Potassium dihydrogen phosphate, sodium hydrogen phosphate and sodium chloride were purchased from Alfa Aesar (USA). Thiolated and fluorescein isothiocyanate (FITC)-terminated deoxyoligonucleotide aptamers were synthesized by Metabion International AG (Germany). Anti-MUC1 DNA sequence: 5-GCA GTT GAT CCT TTG GAT ACC CTG G-$(CH_2)_6$-SH-3′ and 5-FITC-GCA GTT GAT CCT TTG GAT ACC CTG G-$(CH_2)_6$−3′. Chloroform (98.5%), nitric acid (65%), hydrochloric acid (37.5%) and hydroxylamine hydrochloride were purchased from POCh (Poland). All solutions and buffers were prepared using Milli-Q water (resistivity over 18.0 MΩ). UV–Vis–NIR absorption spectra of hollow gold nanoshells were registered using Lambda 25 spectrophotometer (Perkin-Elmer, USA).

A549 (human lung epithelial carcinoma) and MRC−5 (normal human lung fibroblasts) cell lines were obtained from The European Collection of Cell Cultures. MCF−7 (human breast adenocarcinoma) and MCF−10A (human mammary gland) cell lines were purchased from Sigma-Aldrich. For irradiation during phothermal therapy an infrared diode laser module (808 nm, 4 W, Roithner LaserTechnik, RLDH808-4000-5) was applied.

2.2. Hollow gold nanoshells synthesis and surface modification

HGNs were prepared by the galvanic replacement method previously reported by Sun and Xia (2002). Subsequently, the surface of obtained HGNs was modified with anti-MUC1 aptamer. Modification with thiolated DNA was carried out according to protocol described by Braun et al. (2009), which was based on the general procedure of “fast” DNA attachment to citrate-capped nanoparticles at pH 3.0. HGNs purification was performed by centrifugation at 12,000 × *g* for 20 min and resuspending the pellet in 15 mM citrate buffer (pH 7.0) containing 150 mM NaCl. Washing procedure was repeated three times. Finally, HGNs@anti−MUC1 were suspended in 1.2 mL of 15 mM citrate buffer (pH 7.0) with 150 mM NaCl, to reach nominal Au concentration in nanoshells sol of 1 mM. The modified nanoparticles were stored in the darkness at 4 °C and used for further studies within few days.

2.3. Hollow gold nanoshells characterization

Samples of citrate- and ssDNA-modified HGNs were characterized by UV–Vis–NIR spectroscopy in range of 300–1100 nm. Spectra were captured after tenfold dilution of samples in water or 15 mM citrate buffer (pH 7.0) with 150 mM NaCl, respectively. The occurrence of DNA ligands attachment onto GNPs surface was confirmed by the observation of absorption peak assigned to the presence of free DNA in solution (λ_{max} = 260 nm). The drop of intensity in supernatants (compared to solutions of the same theoretical concentration of DNA)

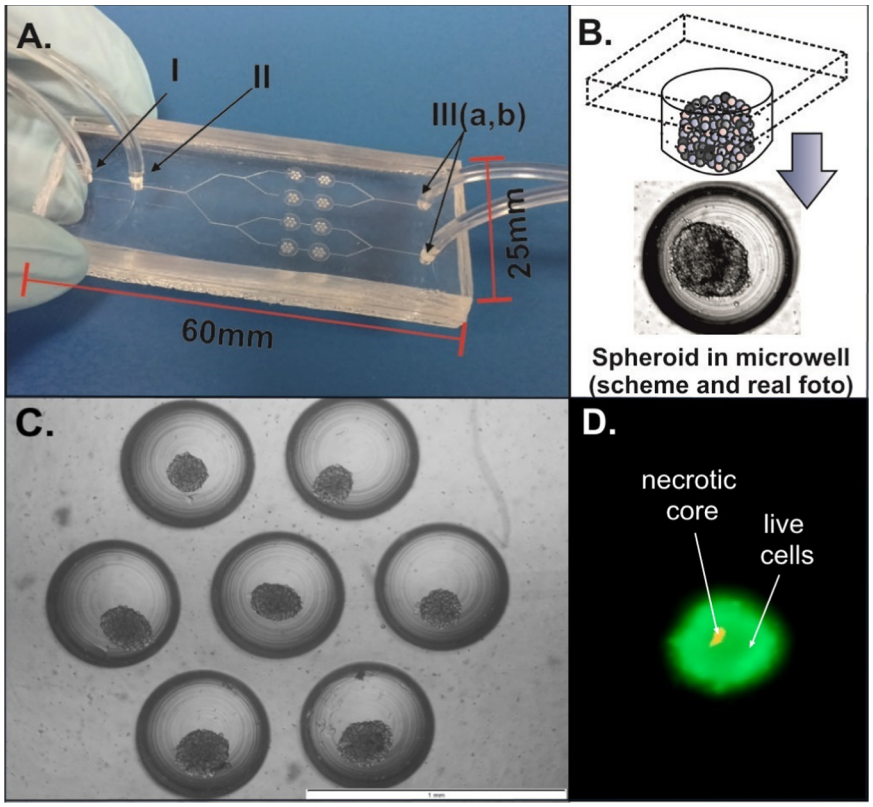

Fig. 1. (A) A photograph of the microsystem: I, III (a, b) – inlets/outlets, II – vent hole. (B) A scheme of spheroid formation and a photograph of a spheroid in microwell. (C) A photograph of a chamber with spheroids in microwells. (D) A photograph of a spheroid stained with calcein-AM (green – live cells) and propidium iodide (red – necrotic cells). (For interpretation of the references to color in this figure legend, the reader is referred to the web version of this article.)

acts as a proof of covalent binding of aptamer to HGNs. Similar methodology was used for monitoring of HGNs purification from the excess of unbound DNA.

In order to determine the temperature behavior of the aptamer-modified nanoparticles, the obtained hollow gold nanoshells solution (in a concentration of 1 mM of Au) was transferred to transparent 96-well plate in volume of 100 µL. Then, the solution was irradiated with laser (power 4 W, 808 nm) for 2 min and temperature of nanoparticles solution was measured using temperature sensor Pt100. Due to better nanoparticles characterization, we also evaluated the repeatability of photothermal changes while nanoparticles solution was repeatedly exposed to irradiation with 30 s interval.

2.4. Microsystem

The microsystem was designed and fabricated using double casting technique according to a method previously described in the literature (Zuchowska et al., 2017). Briefly, the microsystem consisted of two poly (dimethyl siloxane) (PDMS) layers (25 mm × 60 mm) bonded together after their surface activation by oxygen plasma (Fig. 1A). In the bottom layer, microchannels and chambers were fabricated. The microchannels were 100 µm wide and 100 µm deep. The microsystem contained 8 chambers with a diameter of 2700 µm and 100 µm in depth. Each chamber consisted of 7 spherical microwells (with a diameter of 500 µm) (Fig. 1C). The shape of microwells (Fig. 1B) were specially designed and allow to obtain one spheroid in each of them. The second PDMS layer was flat and served as a cover to seal the device. The microsystem architecture (size and chambers arrangements) allowed for the measurements of fluorescence intensity using a standard microplate reader.

2.5. Cell culture

The cells suspension were introduced to the microsystems through inlet I (Fig. 1A) using a peristaltic pump at flow rate 10 µL min^{-1}. Subsequently, the microsystems were incubated for 24 h at 37 °C and 5% CO_2 atmosphere. The spheroid formation was confirmed by microscopic observation (Fig. 1C, D).

2.6. Aptamer uptake

The uptake of fluorescein isothiocyanate (FITC) conjugated with anti-MUC1 aptamer was studied on 2D monolayer and 3D spheroids cell cultures. For 2D studies, the cells were seeded on 96-well plates (with black walls) in density $1{\cdot}10^5$ mL^{-1} and incubated overnight. After cell adhesion to the surface anti-MUC1-FITC conjugates solutions in concentration of 200 nM were introduced to cell cultures and incubated for 24 h. Before the fluorescence intensity measurements, the cells were rinsed twice with PBS. Subsequently, the fluorescence intensity was measured at λ_{em} = 520 nm (λ_{ex} = 493 nm), using BioTek microplate reader.

For 3D spheroid aptamer uptake studies, the spheroids were obtained in the microsystem (Fig. 1D). The anti-MUC1-FITC conjugates solution (200 nM) was introduced to the microsystem and incubated for 24 h with spheroid culture. Then, the microsystem was rinsed with culture medium (without phenol red). In this way, the conjugates that did not accumulate inside cells were removed. Then, microscopic photographs of microwells with spheroids were taken.

2.7. Modified gold nanoshells in vitro cytotoxicity studies (without and after fotoactivation)

2.7.1. Gold nanoshells cytotoxicity without fotoactivation

After formation of the spheroids in the microsystem, aptamer-modified hollow gold nanoshells solution (100 µM) and culture medium (control) were introduced using inlets IIIa and IIIb (Fig. 1A) with a flow rate 4.5 µL min^{-1}. The spheroids cultures were incubated with nanoparticles solution for 24 h and then the viability of the cells was evaluated using Alamar Blue assay. In this test, resazurin is reduced to highly fluorescent resorufin. Fluorescence intensity is proportional to

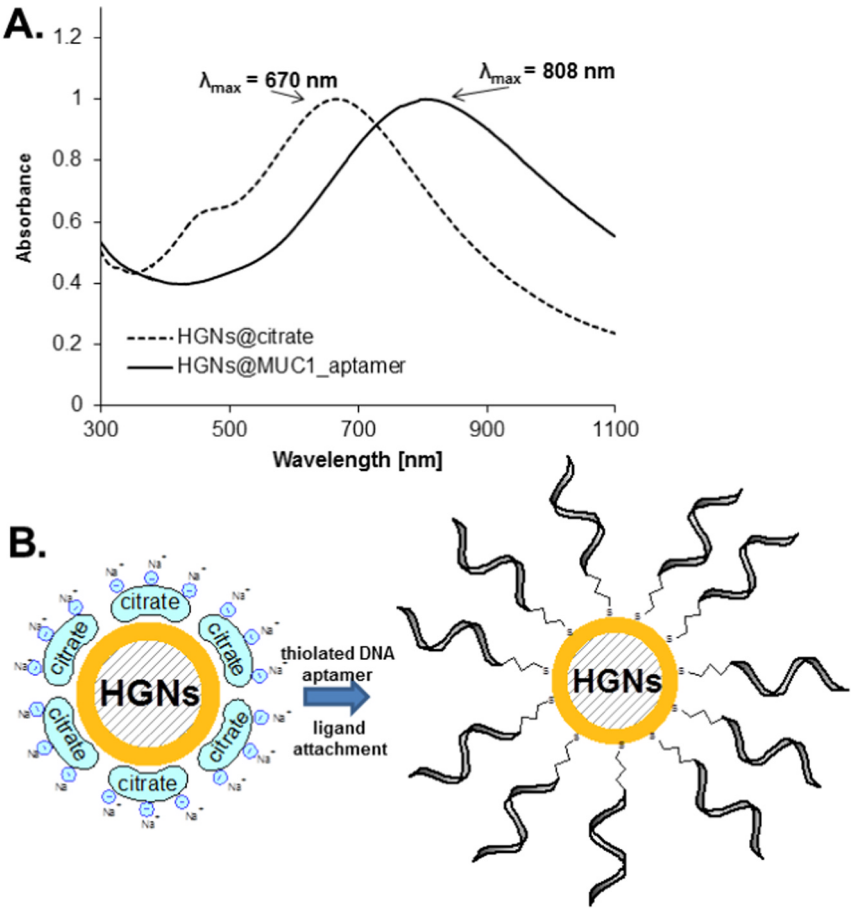

Fig. 2. (A) Absorption spectra of hollow gold nanoshells (HGNs) before (dotted line) and after modification with thiolated ssDNA: anti-MUC1 aptamer (solid line); (B) A scheme of the procedure of HGNs ligand exchange using thiolated DNA aptamer.

the number of living cells. Alamar Blue solution 10% (*v/v*) was prepared in culture medium and introduced into the microsystem using inlet I, flow rate 4.5 μL min^{-1} within 10 min. Then, the spheroids cultures were incubated for 30 min. After the incubation, the fluorescence intensity of resorufin was measured at λ_{ex} = 552 nm, λ_{em} = 582 nm using the microplate reader. After the measurement, the Alamar Blue solution was removed from the microsystem by rinsing with culture medium using a peristaltic pump at a flow rate 4.5 μL min^{-1} within 10 min. The culture was incubated for another 24 h and 72 h and then cells' viability was measured again.

2.7.2. Gold nanoshells cytotoxicity after fotoactivation

The aptamer-modified hollow gold nanoshells solution (in concentration 100 μM of Au) was introduced to the microsystems (through inlet I, flow rate 4.5 μL min^{-1}, within 10 min) and then incubated with spheroids culture for 24 h. Before the irradiation, the spheroids were rinsed with culture medium (without phenol red) in order to remove non-internalized nanoparticles. Then the chambers were irradiated once (PTTx1) or twice with 1 h interval (PTTx2) with 808 nm laser for 5 min. Control sample was not irradiated after incubation with nanoparticles. After the PTT, the microsystem was incubated at 37 °C and 5% CO_2. The viability of the cells was evaluated using Alamar Blue assay 24 h and 48 h after irradiation. Additionally, the changes in spheroids diameter were examined using microscopic observations.

3. Results and discussion

3.1. Hollow gold nanoshells properties

The synthesis of the nanoparticles composed of *quasi*-spherical nanoshell around dielectric core (or hollow interior), apart from a large family of the particles obtained by the controlled growth of nanocrystal facets (e.g. nanorods, nanostars), is one of the most interesting approaches to enable the shift of localized surface plasmon resonance (LSPR) band of gold nanoparticles into NIR region. The facility of controlling the synthesis process can be indicated as a particularly important advantage of the galvanic exchange method. Precise tuning of HGNs geometric dimensions (and thus their optical properties) may be carried out by careful optimization of the size of Ag templates or ratio of Au and Ag precursors. Equally important, both from the point of view of further surface modification and biocompatibility of nanoparticles for biomedical applications, is the selection of the appropriate surface ligand. Capping agents should bind to the Au surface in a reversible manner, giving the opportunity of their replacement by specially designed functional molecules, such as thiolated DNA strands. It is also highly desirable to avoid primary ligands characterized by intrinsic toxicity. Their presence on GNPs surface, which is often caused by resistivity to competitive desorption, may contribute to overall toxic effect of functionalized nanoparticles. Such a problem may be exemplified by gold nanorods, which contain residuals of adsorbed

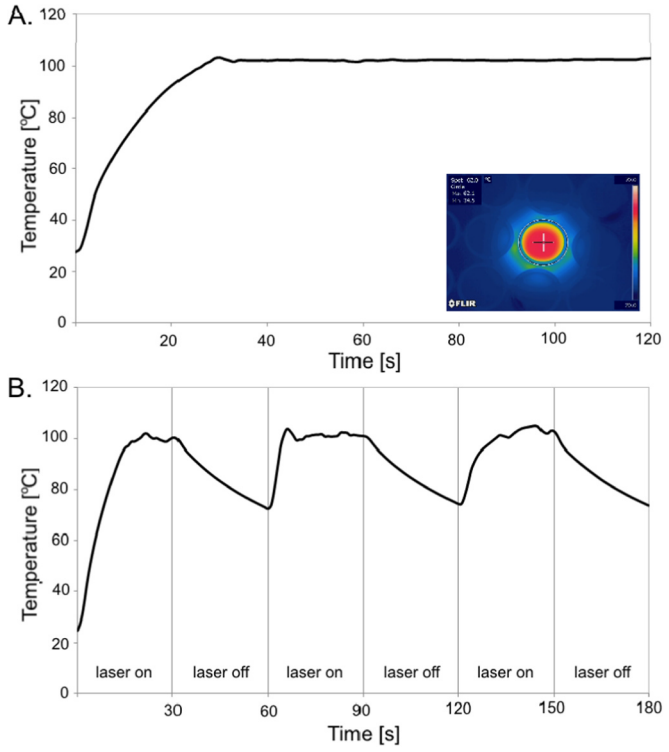

Fig. 3. Temperature changes during 808 nm laser irradiation of hollow gold nanoshells solutions (in a concentration of 1 mM of Au): (A) constant irradiation, (B) 30 s intervals with laser on and off. Additionally thermal imaging infrared photography taken after laser irradiation of hollow gold nanoshells solution (in a well of 96-well plate) is placed in Fig. 3A.

cationic surfactant – CTAB - even after modification with thiolated DNA. Citrate ion appears as ideal ligand, fulfilling both above requirements. Due to the relatively low energy of its interaction with GNPs (~2 kcal/mol (Park and Shumaker-Parry, 2015)), citrate-capped gold nanoparticles have gained great applicability as platforms for further functionalization with thiolated ligands (Melancon et al., 2014). Therefore, citrate-capped HGNs, which combine the biocompatibility, facility of ligand replacement with high absorptivity in NIR region, can also be indicated as promising candidates for PTT (Adams and Zhang, 2016).

The gold nanoparticles applied in this study were designed in order to be accumulated in tumors. The accumulation may be passive or active (Kydd et al., 2017). Passive accumulation is a result of enhanced permeability and retention effect (EPR). This effect occurs in vivo and involves the nanoparticles characterized by size ranging from 10 to 20 nm to 100–200 nm in a diameter (Blocker and Shields, 2018). It was already proven 10–200 times higher number of the nanoparticles may be accumulated in tumor than in normal tissue due to EPR. Active accumulation of the nanoparticles is a result of their targeting using antibodies or aptamers to bind to specific ligands (e.g. proteins). The surface of our nanoparticles was modified with anti-MUC1 aptamer in order to be more likely accumulated by tumor cells that overexpress MUC1. The lower level of this protein occurs in normal cells (see the next paragraph). With regard to these information, our nanoparticles injected into body should be easily accumulated in tumor based on synergistic effect of passive (EPR effect) and active (MUC1 targeting) transport. The nanoparticles size (Salatin et al., 2015; Zhang et al., 2017) will affect not only their concentration in tumor, but also will be essential for optical and photothermal properties of the nanoparticles. Nanoshells size is an important parameter in view of their applications in photothermal therapy.

The scheme of HGNs functionalization together with a photograph

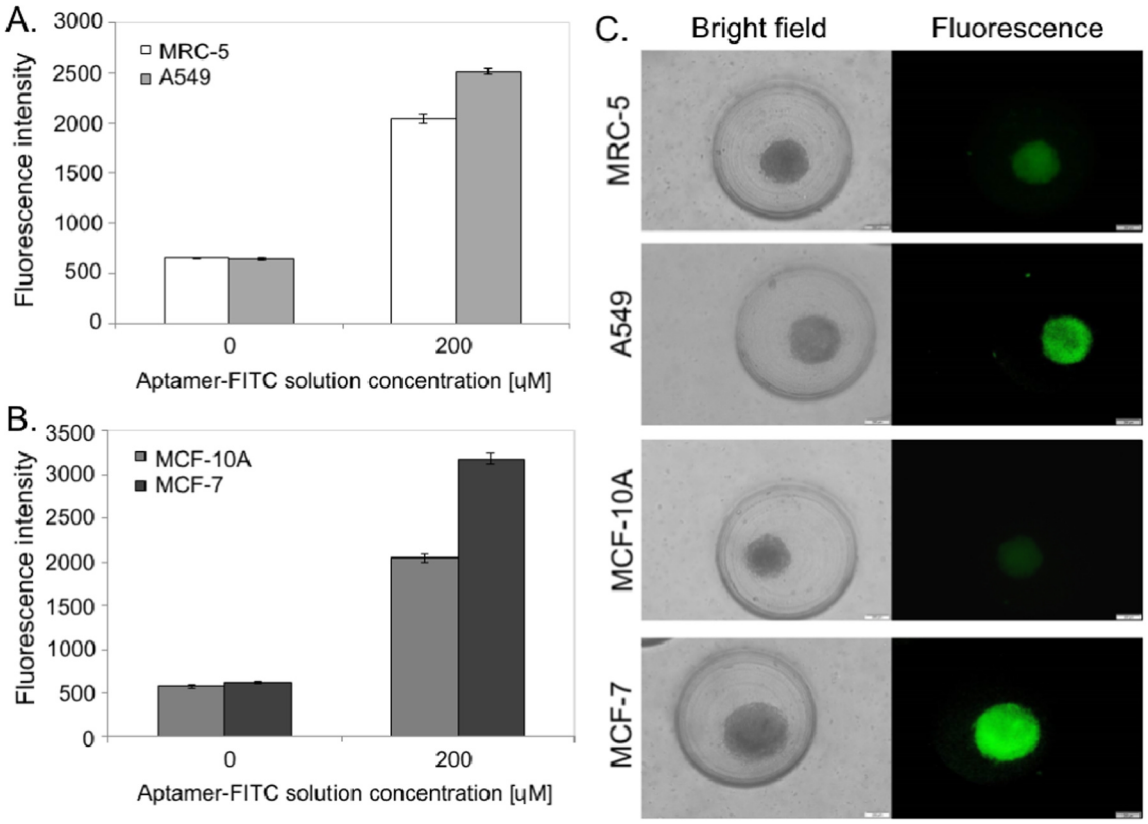

Fig. 4. Results of fluorescence intensity measurements of anti-MUC1 aptamer-FITC conjugates after 24 h incubation with 2D cell cultures: (A) lung MRC-5 and A549 cell lines, (B) breast MCF-10A and MCF-7 cell lines. (C) Pictures of 3D cell cultures after 24 h of incubation with anti-MUC1 aptamer FITC conjugates.

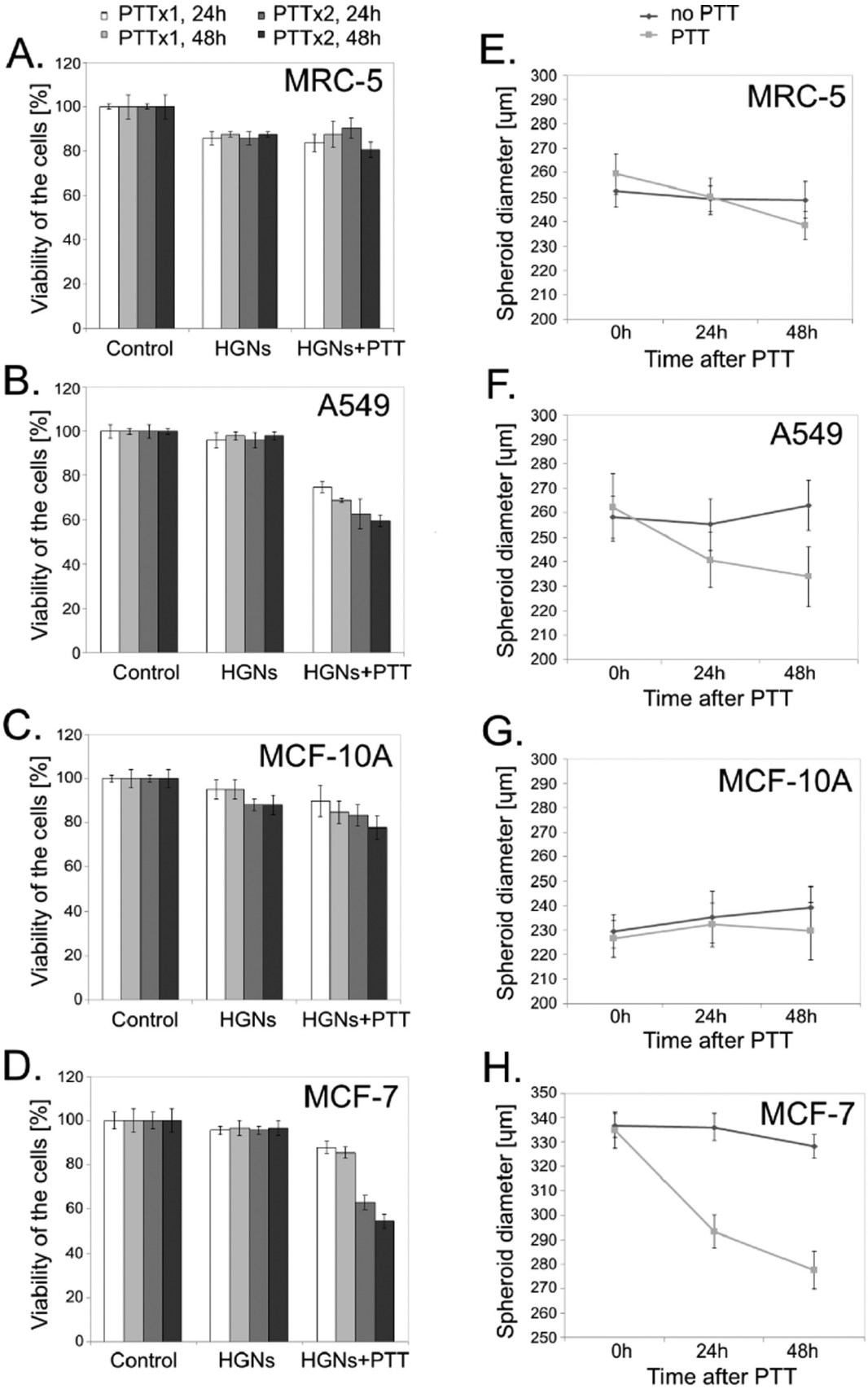

Fig. 5. Viability of the cells after single (PTTx1) or double (PTTx2) irradiation and spheroids' diameters changes (PTTx2) after photothermal therapy using HGNs@ anti-MUC1 aptamer on: (A, E) MRC-5, (B,F) A549, (C,G) MCF-10A, (D,H) MCF-7 multicellular spheroids.

of HGNs@citrate and HGNs@anti−MUC1samples were shown in Fig. 2. Due to the high sensitivity of LSPR band to changes in local environment, HGNs@citrate characterized by absorption maximum at 670 nm were used for DNA aptamers attachment (Fig. 2A). Introduction of thiolated ssDNA onto HGNs surface resulted in a substantial red-shift of LSPR maximum ($\Delta\lambda$ = 135 nm), which is a typical phenomenon observed for plasmonic gold nanostructures (Sun and Xia, 2002). The obtained maximum of absorption at 805 nm was considered satisfactory for further applications of HGNs@anti−MUC1 as photothermally-active agents excited with a laser (wavelength of 808 nm).

The nanoparticles solutions' temperature changes was further measured during laser irradiation (Fig. 3). The constant laser irradiation for 2 min was applied (Fig. 3A). The nanoparticles solution reached the maximal temperature (~100 °C) after ~30 s of irradiation and this temperature remain stable during the whole irradiation time. Additionally, it was examined how repeated irradiation influence on the nanoparticles photothermal properties (Fig. 3B). Triplicated sequence of laser irradiation and cooling showed that nanoparticles solution temperature was raised upto ~100 °C. We observed temperature changes when the laser was turned off. During this time the nanoparticles' solution was slowly cooled down to ~70 °C. Based on these results we confirmed nanoparticles ability to energy transfer (by heat) after laser exposure. This future is essential for photothermally-active agents in PTT.

3.2. Anti-MUC1 aptamer uptake

The uptake of anti-MUC1 aptamer was studied on 2D and 3D cell culture models. The results of fluorescence intensity measurement of the 2D cell cultures incubated with anti-MUC1 aptamer FITC-conjugates are presented in Fig. 4A,B. Both tumor A549 (Masuda et al., 2016) and MCF−7 (Hu et al., 2012) cell lines are characterized by overexpression of MUC1 whereas MRC−5 (Mir et al., 2015) and MCF−10A (Wu et al., 2012) exhibited low levels of MUC1. The obtained results indicated that the anti-MUC1 aptamer uptake was higher in cell lines with higher expression of MUC1 protein. The expression level of various proteins in cells is different and depends on culture model. For example, A549 cells were reported to express higher MUC1 protein levels when cells grow within a complex three-dimensional (3D) microenvironment in comparison to 2D monolayer (Carterson et al., 2005).

The aptamer uptake by multicellular spheroids was additionally evaluated by microscopic observations (Fig. 4C). The tumor spheroids (A549 and MCF–7) were able to internalize higher number of FITC-aptamer conjugates than normal ones (MRC–5 and MCF-10A).

3.3. Photothermal therapy

The results of cytotoxicity studies of HGNs@anti–MUC1 on 3D spheroid cell cultures were presented in Fig. 5A–D. Additionally, effect of cell culture incubation with nanoparticles solution was evaluated by measurements of spheroids' diameters (Fig. 5E-H). After the introduction of surface modified HGNs to spheroids cultures (without laser irradiation), the viability of cells was slightly reduced in comparison to control sample. The viability of MRC-5 and A549 cells was 88% and 98%, respectively. Lower level of metabolic activity was observed for tumor cells (A549 and MCF-7) than for normal ones (MRC-5 and MCF-10A). The size of the spheroids after 24 h incubation with nanoparticles solution remained the same or slightly increased during next 48 h of spheroids culture observation. The initial spheroids size was dependent on the cell line, for example MRC-5 spheroids diameters amounted to ~250 μm whereas MCF-7 spheroids were ~340 μm wide. It was concluded (according to International Standard ISO 10993-5: Tests for Cytotoxicity—In Vitro Methods) that synthetized and modified gold nanoparticles were non-toxic to all examined cell lines (without exposition to laser irradation). To our the best knowledge, cytotoxicity studies of hollow gold nanoshells on multicellular spheroids has not been reported in the literature yet. We find only one report (Pavlovich et al., 2017) that describe the studies on spherical gold nanoparticles toxicity.

The effect of PTT effectiveness performed on normal and tumor spheroids in the microfluidic system was checked (Fig. 5). We evaluated the PTT efficiency with single (PTT x1) or double (PTT x2) laser irradiation. It was observed that double dose of irradiation lead to higher decrease of cell viability, than single exposition to laser irradiation. The obtained cytotoxic effect was depended on the cell line, for normal (lung MRC-5 and breast MCF-10A) cells the viability decreased to 81–90% (PPTx1) and 78–83% (PTTx2). However, the diameter of normal cells spheroids did not change significantly in comparison to control sample (spheroids incubated with HGNs solutions, without laser irradiation). For A549 cell line, single irradiation of spheroids was sufficient to generate cytotoxic effect - after 48 h viability of the cells decreased to 69%. Additional dose of irradiation contributed to further decrease of cell viability (to 59%). The effect of multiple irradiation dose is especially visible in the studies on MCF-7 cell line (about 25% in comparison to single laser exposition). This proves that for each cell line, the optimal parameters of therapeutic procedure should be selected. Based on the performed studies, we found that PTT using HGNs@anti-MUC1 could be an effective and selective cancer treatment method.

4. Conclusions

In this study, hollow gold nanoshells (HGNs) were synthetized using a surfactant-free galvanic replacement method. The HGNs' surface was further modified with an aptamer targeting mucin 1 (MUC1), that is overexpressed on the surface of tumor cells (for example breasts, lungs, colon). We confirmed that anti-MUC1 aptamer conjugated to a fluorescent dye was more effectively accumulated in tumor cells than in normal ones. This phenomenon was observed in the studies on 2D and 3D cultures.

Optical properties of HGNs@anti-MUC1 as well as efficiency of photothermal conversion were examined using UV–Vis spectroscopy and temperature measurements (Pt100). HGNs@anti-MUC1 absorption maximum was located in NIR region. The nanoparticles solutions were effectively heated up during 808 nm laser irradiation. They were also stable after triple rounds of heating and cooling. Due to their excellent properties, HGNs@anti-MUC1 were subsequently applied for targeted photothermal therapy (PTT) on 3D model of tumor in microfluidic condition. Application of *lab-on-a*-chip microfluidic systems allowed to create conditions which better mimics in vivo (e.g. laminar flow, transport of nutrients and oxygen by diffusion).

In this original studies, we cultured 3D multicellular spheroids, performed laser irradiation and evaluate effectiveness of therapeutic procedure using the microfluidic device. Such a research has not been reported in the literature yet. The studies were conducted on two tumor (lung A549 and breast MCF-7) and two normal (lung MRC-5 and breast MCF–10A) cell lines. When no laser irradiation was applied, HGNs@anti-MUC1 nanoparticles were non-toxic towards both tumor and normal spheroids. The efficiency of PTT was evaluated after single (PTTx1) and double (PTTx2) laser irradiation. In this way, we compare effectiveness two strategies of conducting therapy. Double irradiation provided better efficiency of PTT-induced cytotoxicity towards tumor spheroids. HGNs@anti–MUC1 nanoparticles-guided photothermal therapy did not affect normal cells' viability to such an extent as tumor cells'. This work contribute to expanding knowledge in the field of cancer therapy methods. Our studies creates perspective for development of efficient, non-invasive and selective anti-cancer therapies.

Appendix A. Supporting information

Supplementary data associated with this article can be found in the online version at doi:10.1016/j.bios.2018.10.069.

References

Adams, S., Zhang, J.Z., 2016. Coord. Chem. Rev. 320–321, 18–37.
Ahmed, K., Tabuchi, Y., Kondo, T., 2015. Apoptosis 20, 1114–1119.
Azhdarzadeh, M., Atyabi, F., Saei, A.A., Varnamkhasti, B.S., Omidi, Y., Fateh, M., Ghavami, M., Shanehsazzadeh, S., Dinarvand, R., 2016. Colloids Surf. B Biointerfaces 143, 224–232.
Babiker, H.M., McBride, A., Newton, M., Boehmer, L.M., Drucker, A.G., Gowan, M., Cassagnol, M., Camenisch, T.D., Anwer, F., Hollands, J.M., 2018. Crit. Rev. Oncol. Hematol. 126, 186–200.
Blocker, S.J., Shields, A.F., 2018. Mol. Imaging Biol. 20, 340–351.
Braun, G.B., Pallaoro, A., Wu, G., Missirlis, D., Zasadzinski, J.A., Tirrell, M., Reich, N.O., 2009. ACS Nano 3, 2007.
Carterson, A.J., Höner zu Bentrup, K., Ott, C.M., Clarke, M.S., Pierson, D.L., Vanderburg, C.R., Buchanan, K.L., Nickerson, C.A., Schurr, M.J., 2005. Infect. Immun. 73, 1129–1140.
Cavo, M., Caria, M., Pulsoni, I., Beltrame, F., Fato, M., Scaglione, S., 2018. Sci. Rep. 8, 5333.
Chifor, R., Badea, I., Avram, R., Chifor, I., Badea, M.E., Todea, D.C., Podoleanu, A.G., Duma, V.-.F., 2016. (Eds.), International Society for Optics and Photonics: p. 96700A.
Crawford, B., Shammas, R., Fales, A., Brown, D., Hollenbeck, S., Vo-Dinh, T., Devi, G., 2017. Int. J. Nanomed. 12, 6259–6272.
Datta, N.R., Gómez Ordóñez, S., Gaipl, U.S., Paulides, M.M., Crezee, H., Gellermann, J., Marder, D., Puric, E., Bodis, S., 2015. Cancer Treat. Rev. 41, 742–753.
Fennema, E., Rivron, N., Rouwkema, J., van Blitterswijk, C., de Boer, J., 2013. Trends Biotechnol. 31, 108–115.
Gai, S., Yang, G., Yang, P., He, F., Lin, J., Jin, D., Xing, B., 2018. Nano Today 19, 146–187.
Gonçalves, D.P.N., Rodriguez, R.D., Kurth, T., Bray, L.J., Binner, M., Jungnickel, C., Gür, F.N., Poser, S.W., Schmidt, T.L., Zahn, D.R.T., Androutsellis-Theotokis, A., Schlierf, M., Werner, C., 2017. Acta Biomater. 58, 12–25.
Gontran, E., Juchaux, M., Deroulers, C., Kruglik, S., Huang, N., Badoual, M., Seksek, O., 2018. J. Appl. Polym. Sci. 135, 46287.
Hori, S., Herrera, A., Rossi, J., Zhou, J., 2018. Current advances in aptamers for cancer diagnosis and therapy. Cancers 10, 9.
Hu, Y., Duan, J., Zhan, Q., Wang, F., Lu, X., Yang, X.-D., 2012. PLoS One 7, e31970.
Kalinowska, D., Tokarska, K., Grabowska-Jadach, I., Dybko, A., Brzozka, Z., 2018. Lab-on-a-chip Systems for Cellomics—Materials and Technology. Springer International Publishing, pp. 23–53.
Kydd, J., Jadia, R., Velpurisiva, P., Gad, A., Paliwal, S., Rai, P., 2017. Pharmaceutics 9, 46.
Li, X., Zhou, J., Dong, X., Cheng, W.-Y., Duan, H., Cheung, P.C.K., 2018. J. Agric. Food Chem. 66, 4091–4098.
Lopatynskyi, A.M., Malymon, Y.O., Lytvyn, V.K., Mogylnyi, I.V., Rachkov, A.E., Soldatkin, A.P., Chegel, V.I., 2017. Plasmonics 1–11.
Mantso, T., Goussetis, G., Franco, R., Botaitis, S., Pappa, A., Panayiotidis, M., 2016. Semin. Cancer Biol. 37–38, 96–105.
Martínez, O., Bellard, E., Golzio, M., Mechiche-Alami, S., Rols, M.-P., Teissié, J., Ecochard, V., Paquereau, L., 2014. Nucleic Acid. Ther. 24, 217–225.
Masuda, M., Kawakami, S., Wijagkanalan, W., Suga, T., Fuchigami, Y., Yamashita, F., Hashida, M., 2016. Biol. Pharm. Bull. 39, 1734–1738.
Melancon, M.P., Zhou, M., Zhang, R., Xiong, C., Allen, P., Wen, X., Huang, Q., Wallace, M., Myers, J.N., Stafford, R.J., Liang, D., Ellington, A.D., Li, C., 2014. ACS Nano 8, 4530–4538.
Min, J., Hye, L., Seo, I., Hyuk, J., Bong, B., Chung, G., 2017. Electrophoresis 38, 1318–1324.
Mir, T.A., Yoon, J.-H., Gurudatt, N.G., Won, M.-S., Shim, Y.-B., 2015. Biosens. Bioelectron. 74, 594–600.
Mokwena, M.G., Kruger, C.A., Ivan, M.-T., Heidi, A., 2018. Photo. Photodyn. Ther. 22, 147–154.
Nabavinia, M.S., Gholoobi, A., Charbgoo, F., Nabavinia, M., Ramezani, M., Abnous, K., 2017. Med. Res. Rev. 37, 1518–1539.
Norouzi, H., Khoshgard, K., Akbarzadeh, F., 2018. Lasers Med. Sci. 33, 917–926.
Park, J.-W., Shumaker-Parry, J.S., 2015. ACS Nano 9, 1665–1682.
Pavlovich, E., Volkova, N., Yakymchuk, E., Perepelitsyna, O., Sydorenko, M., Goltsev, A., 2017. Nanoscale Res. Lett. 12, 494.
S, Y., Xia, Y., 2002. Anal. Chem. 74, 5297–5305.
Salatin, S., Maleki Dizaj, S., Yari Khosroushahi, A., 2015. Cell Biol. Int. 39, 881–890.
Siegel, R.L., Miller, K.D., Jemal, A., 2018. Cancer statistics, 2018. CA Cancer J. Clin. 68, 7–30.
Singh, S., Jha, P., Singh, V., Sinha, K., Hussain, S., Singh, M.K., Das, P., 2016. Integr. Biol. 8, 1040–1048.
Wang, J., Zhu, C., Han, J., Han, N., Xi, J., Fan, L., Guo, R., 2018. ACS Appl. Mater. Interfaces 10, 12323–12330.
Weiswald, L.-B., Bellet, D., Dangles-Marie, V., 2015. Neoplasia 17, 1–15.
Wu, P., Gao, Y., Zhang, H., Cai, C., 2012. Anal. Chem. 84, 7692–7699.
Xia, X., Xia, Y., 2014. Front. Phys. 9, 378–384.
Yang, C., Murray, J.L., Ibrahim, N.K., 2018. Elsevier 225–240.
Zhang, J., Tang, H., Liu, Z., Chen, B., 2017. Int. J. Nanomed. 12, 8483–8493.
Zuchowska, A., Jastrzebska, E., Chudy, M., Dybko, A., Brzozka, Z., 2017. Anal. Chim. Acta 990, 110–120.